RESEARCH ARTICLE SUMMARY

PLANETARY SCIENCE

Cratering on Ceres: Implications for its crust and evolution

H. Hiesinger,* S. Marchi, N. Schmedemann, P. Schenk, J. H. Pasckert, A. Neesemann, D. P. O'Brien, T. Kneissl, A. I. Ermakov, R. R. Fu, M. T. Bland, A. Nathues, T. Platz, D. A. Williams, R. Jaumann, J. C. Castillo-Rogez, O. Ruesch, B. Schmidt, R. S. Park, F. Preusker, D. L. Buczkowski, C. T. Russell, C. A. Raymond

INTRODUCTION: Thermochemical models have predicted that the dwarf planet Ceres has, to some extent, formed a mantle. Moreover, due to viscous relaxation, these models indicate that Ceres should have an icy crust with few or no impact craters. However, the Dawn spacecraft has shown that Ceres has elevation excursions of ~15 km, cliffs, graben, steep-sided mountains, and a heavily cratered surface.

RATIONALE: We used Dawn's Framing Camera to study the morphology, size frequency, and spatial distribution of the craters on Ceres. These data allow us to infer the structure and evolution of Ceres' outer shell.

RESULTS: A large variety of crater morphologies are present on Ceres, including bowl-shaped craters, polygonal craters, floor-fractured craters, terraces, central peaks, smooth floors, flowlike features, bright spots, secondary craters, and crater chains. The morphology of some impact craters is consistent with water ice in the subsurface. Although this might have favored relaxation, there are also large unrelaxed craters. The transition from bowl-shaped simple craters to modified complex craters occurs at diameters of about 7.5 to 12 km. Craters larger than 300 km are absent, but low-pass filtering of the digital elevation model suggests the existence of two quasi-circular depressions with diameters of ~570 km (125.56°E and 19.60°N) and ~830 km (24.76°W and 0.5°N). Craters are heterogeneously distributed across Ceres' surface, with more craters in the northern versus the southern hemisphere. The lowest crater densities are associated with large, well-preserved southern hemisphere impact craters such as Urvara and Yalode. Because the low crater density (LCD) terrain extends across a large latitude range in some cases (e.g., Urvara and Yalode: ~18°N and 75°S; Kerwan: ~30°N and 46°S), its spatial distribution is inconsistent with simple relaxation driven by warmer equatorial temperatures. We instead propose that impact-driven resurfacing is the more likely LCD formation process, although we cannot completely rule out an internal (endogenic) origin. We applied two different methodologies to derive absolute model ages from observed crater size-frequency distributions. The lunar-derived model adapts the lunar production and chronology functions to impact conditions on Ceres, taking into account impact velocities, projectile densities, current collision probabilities, and surface gravity. The asteroid-derived model derives a production function by scaling the directly observed object size-frequency distribution from the main asteroid belt (extended to sizes <5 km by a collisional model) to the resulting size-frequency distribution of cerean craters, using similar cerean target parameters as the lunar-derived model. By dating a smooth region associated with the Kerwan crater, we determined absolute model ages of 550 million and 720 million years, depending on which chronology model is applied.

ON OUR WEBSITE

Read the full article at http://dx.doi.org/10.1126/science.aaf4759

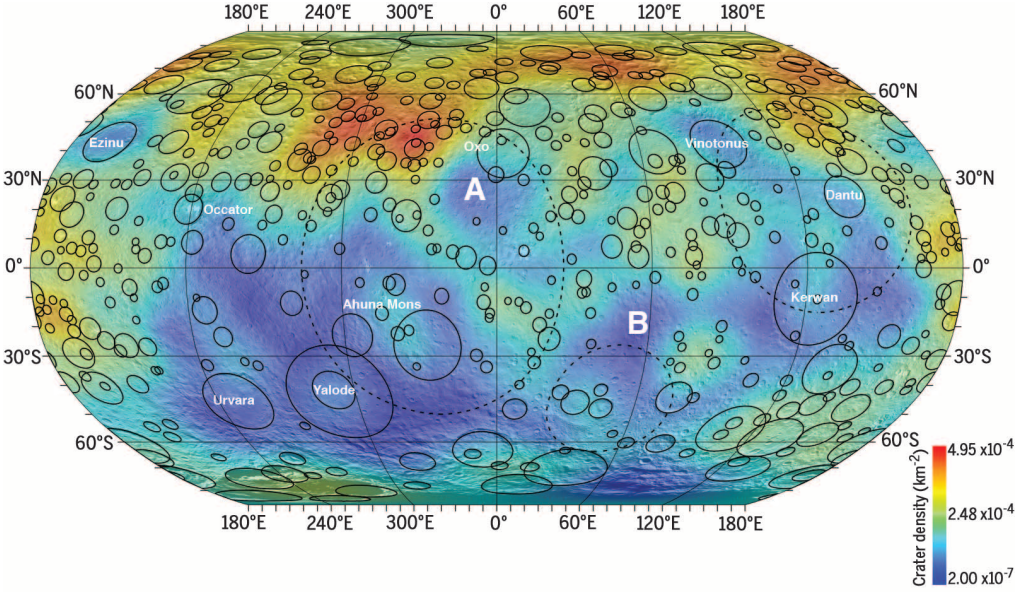

Spatial density of craters larger than 20 km on Ceres. Crater rims are shown as black solid circles. Blue indicates areas with LCDs; yellow and red represent more highly cratered areas. The smallest dashed ellipse denotes the idealized former rim of an extremely degraded impact crater at 48.9°E and 44.9°S, which is barely recognizable in imagery but apparent from the global digital elevation model. Also shown as dashed circles are the outlines of two large putative basins. Unambiguously recognized basins >300 km in diameter are missing, and there are several areas with LCDs associated with large impact craters (e.g., Yalode, Urvara, Kerwan, Ezinu, Vinotonus, Dantu, and two unnamed craters northeast and southeast of Oxo). Areas A and B are topographic rises with central depressions that also show LCDs.

CONCLUSION: Crater morphology and the simple-to-complex crater transition indicate that Ceres' outer shell is likely neither pure ice nor pure rock but an ice-rock mixture that allows for limited relaxation. The heterogeneous crater distribution across the surface indicates crustal heterogeneities and a complex geologic evolution of Ceres. There is evidence for at least some geologic activity occurring in Ceres' recent history. ■

The list of author affiliations is available in the full article online.
*Corresponding author. Email: hiesinger@uni-muenster.de
Cite this article as H. Hiesinger *et al.*, *Science* 353, aaf4759 (2016). DOI: 10.1126/science.aaf4759

RESEARCH ARTICLE

PLANETARY SCIENCE

Cratering on Ceres: Implications for its crust and evolution

H. Hiesinger,[1]* S. Marchi,[2] N. Schmedemann,[3] P. Schenk,[4] J. H. Pasckert,[1] A. Neesemann,[3] D. P. O'Brien,[5] T. Kneissl,[3] A. I. Ermakov,[6] R. R. Fu,[6] M. T. Bland,[7] A. Nathues,[8] T. Platz,[8] D. A. Williams,[9] R. Jaumann,[10,3] J. C. Castillo-Rogez,[11] O. Ruesch,[12] B. Schmidt,[13] R. S. Park,[11] F. Preusker,[10] D. L. Buczkowski,[14] C. T. Russell,[15] C. A. Raymond[11]

Thermochemical models have predicted that Ceres, is to some extent, differentiated and should have an icy crust with few or no impact craters. We present observations by the Dawn spacecraft that reveal a heavily cratered surface, a heterogeneous crater distribution, and an apparent absence of large craters. The morphology of some impact craters is consistent with ice in the subsurface, which might have favored relaxation, yet large unrelaxed craters are also present. Numerous craters exhibit polygonal shapes, terraces, flowlike features, slumping, smooth deposits, and bright spots. Crater morphology and simple-to-complex crater transition diameters indicate that the crust of Ceres is neither purely icy nor rocky. By dating a smooth region associated with the Kerwan crater, we determined absolute model ages (AMAs) of 550 million and 720 million years, depending on the applied chronology model.

Ceres is the largest (~940-km diameter) and most massive object in the asteroid belt and, as a protoplanet, possibly holds clues to our understanding of the early solar system history (*1*). Pre-Dawn mission studies, mostly based on data acquired by Earth-based telescopes and the Hubble Space Telescope, have revealed several notable results. For example, some pre-Dawn geophysical models have predicted that Ceres is a differentiated body with a silicate-rich core and a water-rich shell (*2*–*5*), resulting in a hydrostatic shape and relatively rapid viscous relaxation (i.e., removal) of topographic features, including impact craters (*4*). In addition, early spectral data of Ceres were interpreted as evidence for water in clay minerals, brucite, carbonates, iron-rich serpentine, and ammoniated phyllosilicates (*6*–*10*). Volatile-rich CI and CM chondrites are probably the best meteoritic analog materials for Ceres (*11*, *12*). Dawn is the first spacecraft to visit Ceres and closely observe its surface from an orbit as low as 850 km in radius (*5*). Although Dawn carries several instruments, including a Visible and Infrared Spectrometer (VIR) (*13*) and a Gamma Ray and Neutron Detector (GRaND) (*14*), in this study we mostly rely on images of the Framing Camera (FC) (*15*), which observes the cerean surface in one broadband clear filter (400 to 1100 nm) and seven narrowband color filters (438, 555, 653, 749, 829, 917, and 965 nm).

[1]Institut für Planetologie, Westfälische Wilhelms-Universität, Münster, Germany. [2]Southwest Research Institute, Boulder, CO 80302, USA. [3]Institute of Geological Sciences, Freie Universität Berlin, Berlin, Germany. [4]Lunar and Planetary Institute, Houston, TX 77058, USA. [5]Planetary Science Institute, Tucson, AZ 85719, USA. [6]Massachusetts Institute of Technology, Cambridge, MA 02139, USA. [7]U.S. Geological Survey, Astrogeology Science Center, Flagstaff, AZ 86001, USA. [8]Max-Planck Institute for Solar System Research, Göttingen, Germany. [9]Arizona State University, Tempe, AZ 85281, USA. [10]German Aerospace Center (DLR), Berlin, Germany. [11]Jet Propulsion Laboratory, California Institute of Technology, Pasadena, CA 91109, USA. [12]NASA Goddard Space Flight Center, Greenbelt, MD 20771, USA. [13]Georgia Institute of Technology, Atlanta, GA 30332, USA. [14]John Hopkins Applied Physics Laboratory, Laurel, MD 20723, USA. [15]Department of Earth and Space Sciences, University of California, Los Angeles, CA 90095, USA.
*Corresponding author. Email: hiesinger@uni-muenster.de

Crater morphology

We studied FC (*15*) images with a spatial resolution of up to 137 m per pixel that reveal a rich inventory of morphologic features, such as cliffs, graben, steep-sided mountains, and craters. In fact, FC images show a large number and variety of crater morphologies, including bowl-shaped craters, polygonal craters, floor-fractured craters, crater terraces, central peaks, smooth crater floors, craters with flowlike features, and secondary craters and crater chains (Fig. 1). The morphologies of <30- to 40-km-diameter craters on Ceres are indistinguishable from craters on mid-sized icy moons of Saturn (e.g., Dione and Tethys) (*16*). At Ceres, floor-filling smooth material is commonly observed in craters >40 km but has not been reported from mid-sized icy moons (*16*). The smooth deposits occur at various elevations, embay other crater material, and might represent mixed mobilized impact melt or debris, impact-triggered volcanism, or postimpact melting. At some crater walls, we observe flowlike deposits with steep lobe fronts and sides, as well as striations in downslope direction that we interpret as evidence for mobilization of crustal material in the presence of ice (*17*). Craters larger than 40 km exhibit additional morphologies not observed at smaller craters—for instance, central pits, possible pit floors, and floor fractures. Central pits similar to pits on Ganymede and Callisto occur preferentially in craters >75 km. These crater morphologies are described in more detail in a companion paper by Buczkowski *et al.* (*17*). On the basis of their morphological characteristics, we propose that craters on Ceres were formed in a relatively weak target (i.e., much weaker than intact or partially fractured crystalline rock) when compared with Vesta or the Moon, consistent with the presence of ice (*2*–*4*, *18*).

Several pre-Dawn thermochemical models have predicted that Ceres is, to some extent, a differentiated body that potentially has a silicate-rich core and a water-rich shell (*2*–*5*, *18*–*20*). The more differentiated structure models would allow for a hydrostatic shape and relatively rapid viscous relaxation of craters (*4*). The predicted paucity of craters resulted from the assumption of a 10- to 100-km-thick surface-ice layer and relatively high surface temperatures, which allow for rapid viscous relaxation. Image-based digital elevation models (DEMs) (*21*–*23*) help determine the degree of differentiation by revealing elevation differences of ~15 km, indicating that Ceres' shell may contain less ice than predicted by the more differentiated models. If Ceres contains an ice-dominated layer, it was predicted that even small craters would relax within 10 million to 100 million years (My) (assuming relatively warm temperatures of 180 K) and that pristine craters could survive only near the poles (*4*). This is not consistent with Dawn observations.

Improved temperature models (*24*) suggest lower equatorial temperatures of 155 K, and <110 K at latitudes higher than ~80°, slowing viscous relaxation and increasing the survival time of craters. An undifferentiated rocklike model, in which water is entirely bound to minerals in the form of hydrated salts and silicates (*25*), predicts that relaxation of craters is not expected (*4*). However, Castillo-Rogez (*19*) argued that the undifferentiated model is not realistic from a thermal evolution standpoint, and it is also inconsistent with Dawn observations of moderately relaxed craters. We find that, unlike in (*4*), viscous relaxation is relevant only at scales of several hundreds of kilometers. Among Ceres' few features of that size is the Kerwan impact crater (284 km), which appears partially relaxed because of the absence of a central peak, the subdued rim, the gently-sloped smooth floor, and the lower crater density compared with the surrounding terrain. Although we cannot completely exclude geologic processes—such as degradation from subsequent impact cratering or cryovolcanism—that might have operated locally or regionally in the Kerwan area, we favor viscous relaxation as the most likely origin of this crater's unusual morphology. This is because of Kerwan's position close to the warm equator, its size and morphology, as well as results of viscoelastic finite element models of Bland *et al.* (*26*). In addition, Kerwan is located in an area with a low crater density (LCD), making degradation by subsequent impact craters less likely. Similarly, we did not find unambiguous

evidence for cryovolcanic resurfacing of Kerwan. In contrast to Kerwan, Dawn DEMs indicate that the majority of Ceres' craters are deep. For example, Vinotonus (140 km, 94.8°E and 43.1°N), Ezinu (120 km, 195.4°E and 43.2°N), Urvara (170 km, 248.6°E and 46.3°S), Yalode (267 km, 292.5°E and 42.3°S), and several other large craters have depths of >4 km. They are deeper than similar-sized fresh lunar craters (*27*) and modestly shallower than fresh craters on Tethys (*16*). Further, Ceres' craters are much deeper than the completely flattened craters predicted by Bland (*4*) in this size range for a pure ice layer. Thus, Dawn's observations of preserved and relaxed craters, along with Ceres' shape (*5*), are inconsistent with a pure rocky outer shell. Clearly, viscous relaxation has played a limited but important role in subduing some craters. The lack of observed relaxation for craters smaller than Kerwan indicates that any outer shell has a rheology much stronger than that of pure water ice (*4*). Thus, Ceres' outer shell is probably neither pure ice nor pure rock but an ice-rock mixture that allows for limited relaxation at the longest wavelengths. In addition, differences in relaxation across the surface possibly indicate spatial variations in the ice content of the outer layer on Ceres.

Crater morphometry

A second test of the proposed thermochemical models is the transition diameter from simple (bowl-shaped) to complex (e.g., central peaks, terraces, rings) crater morphology. Provided that Ceres is a predominantly icy body with a gravity of 0.28 m/s^2 (*5*), it has been predicted that the transition would occur at a diameter of ~16 km; it would occur at ~50 km for a rocky body (*4*). In particular, Bland (*4*) suggested that a transition diameter of 10 to 20 km would be consistent with a thick icy layer, whereas a diameter of more than 20 km would support the undifferentiated model of Zolotov (*25*). To determine the simple-to-complex transition diameter, we selected ~160 well-preserved craters on the basis of their crisp morphology and the absence of obvious post-impact erosion or modification. Two criteria were used: (i) inflection in the depth-diameter curve

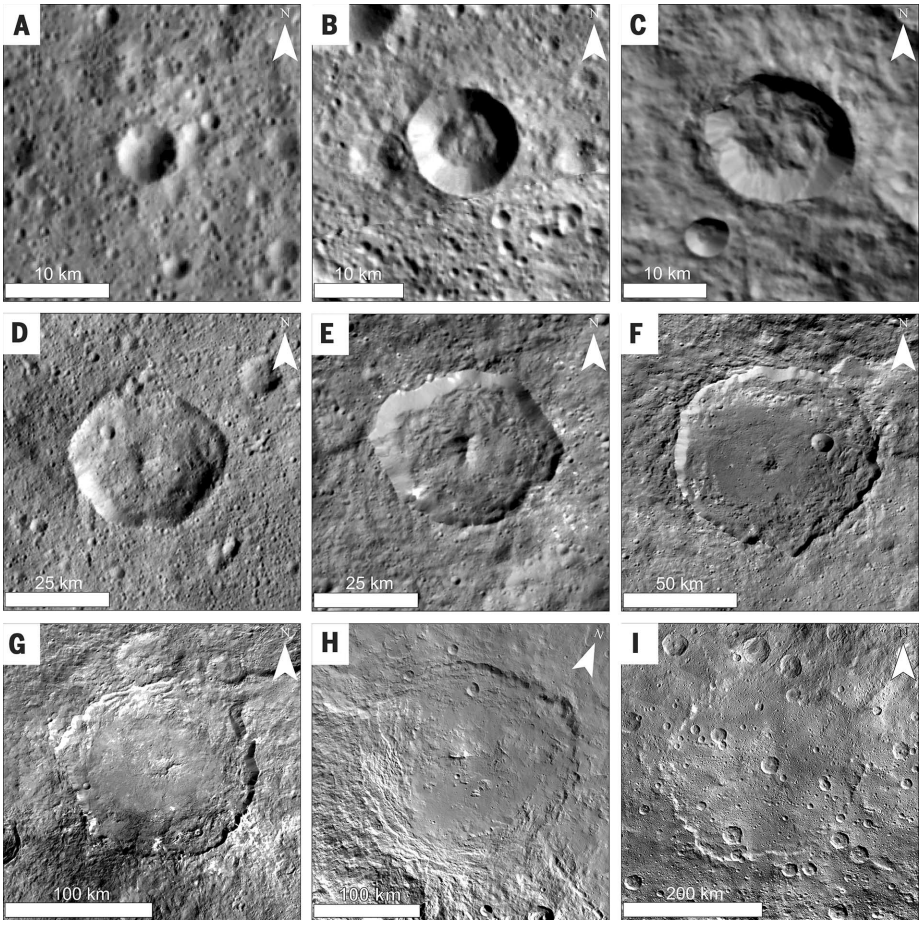

Fig. 1. Morphologies of impact craters on Ceres. (**A**) Unnamed 6-km simple bowl-shaped crater (105°E and 3°N). (**B**) Unnamed 12.5-km modified simple crater (161.7°E and 13°S) with mass-wasting deposits on the floor. (**C**) Unnamed 16- to 18.8-km complex crater (279°E and 23°S) with possible terraces and evidence for mass wasting on the floor and walls. Mass-wasting deposits form ridges on the crater floor. (**D**) Unnamed 34- to 37-km complex crater with central peak (108°E and 10°N). (**E**) Achita, a 41-km polygonal complex crater (65.8°E and 25.8°N) with mass-wasting ridges on the floor. (**F**) Gaue crater (84 km, 85.9°E and 30.9°N) showing multiple terraces, a central pit, a smooth and flat floor, and a small peak close to the central pit. (**G**) Dantu crater (125 km, 137.8°E and 24.4°N), with concentric terraces, a possible peak ring structure or central pit, a smooth and flat floor, and considerable albedo variations at the southwestern rim. (**H**) Urvara crater (170 km, 248.6°E and 46.3°S), with concentric terraces, a small elongated central peak, a smooth and flat floor, and a relaxed morphology. (**I**) Kerwan crater (284 km, 123.6°E and 10.9°S) shows a partially relaxed morphology and does not have a central peak but instead a central depression. This crater's rim is subdued, and the floor is gently sloped and almost completely covered by smooth material with a lower crater density than the surrounding terrain. Arrowheads point north.

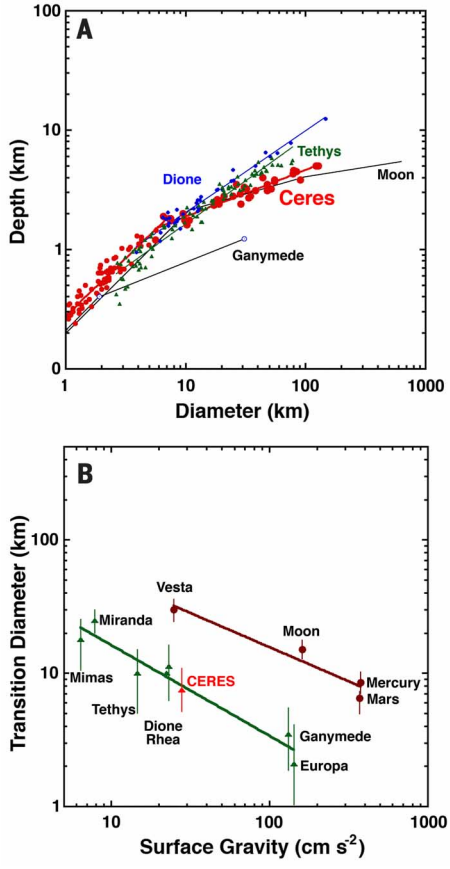

Fig. 2. Simple-to-complex transition diameters of impact craters on Ceres and selected icy moons and rocky bodies. (**A**) Simple-to-complex crater transitions (i.e., those with more than 50% modified floors) on Ceres (small red circles represent simple craters; large red circles represent complex craters) occur at diameters of 7.5 to 12 km. The depth/diameter ratios of the dry Moon (black line) and those of the icy bodies Dione (blue circles), Tethys (green triangles), and Ganymede (blue open circles) are shown for comparison. (**B**) The transition diameters to complex craters scale inversely with surface gravity of the respective body. Taking into account its surface gravity, the depth/diameter ratio of Ceres (red triangle) follows the same trend as other icy bodies (green triangles). The transition diameters to complex craters of rocky bodies (brown circles) are shown for comparison.

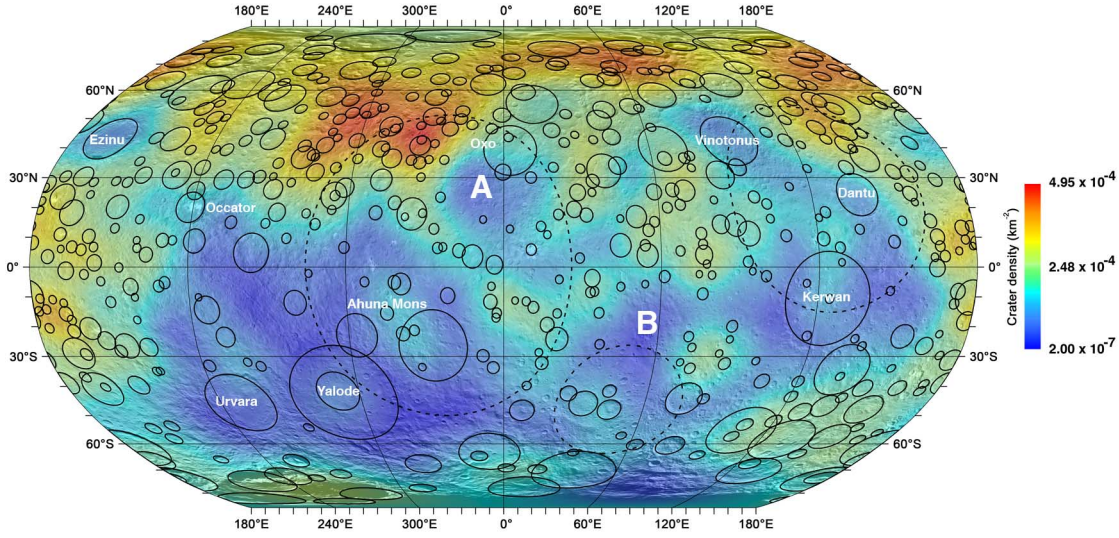

Fig. 3. Spatial density of >20-km craters on Ceres. Crater rims are shown as black solid circles. Blue indicates areas with LCDs; yellow and red represent highly cratered areas. The smallest dashed ellipse marks the idealized former rim of an extremely degraded impact crater at 48.9°E and 44.9°S, which is barely recognizable in the FC clear filter data but visible in the global DEM. Also shown as dashed circles are the outlines of two large putative basins. Unambiguously recognized basins with diameters >300 km are missing, and there are several areas with LCDs associated with large impact craters (e.g., Yalode, Urvara, Kerwan, Ezinu, Vinotonus, Dantu, and two unnamed craters northeast and southeast of Oxo). Areas A and B are topographic rises with central depressions (described in the text) that also show LCDs.

and (ii) the morphologic transition from simple (relatively unmodified) bowl-shaped craters to those with modified floors. Our criteria for the latter was when modified floors exceed 50% of the crater diameter and when the number of craters in a size bin exceeds 50% occurrence of modified complex crater floors. These are the same criteria used for comparison to icy satellites (*28*). We used the current High-Altitude Mapping Orbit (HAMO) topographic map of Ceres, which has an effective horizontal resolution of ~137 m and a vertical sensitivity of 10 m (*23*), to measure crater depths. For craters less than ~8 km in diameter, we determined the crater depths from shadow measurements. We found that the transition from bowl-shaped simple craters to modified simple craters (based on observations of floor-fill material and on the inflection in the depth-diameter curve) occurs at about 7.5 to 12 km. These results are generally similar to those of other icy bodies with similar gravity, such as Tethys (~10 km) and Dione (~10 to 12.5 km), when measured with the same criteria (Fig. 2A). Assuming that simple-to-complex transition diameters scale inversely with gravity (*29*) (Fig. 2B), we can independently calculate the Ceres simple-to-complex transition diameter following the approach used in (*30*) and (*31*), which gives the simple-to-complex transition diameter as $2g_{Ganymede}/g_{Ceres}$ (g, gravity). Assuming a gravity of 1.428 m/s^2 for Ganymede (*32*) and of 0.28 m/s^2 for Ceres (*5*), this yields a simple-to-complex transition on Ceres at ~10.3 km. In contrast, if Ceres is primarily a rocky body, then Ceres' transition diameter could be near 50 km (*4*), as can be obtained by the extrapolation of the values associated with silicate planets from (*29*). Thus, these independent calculations support the fact that Ceres has a crust made of an ice-rock

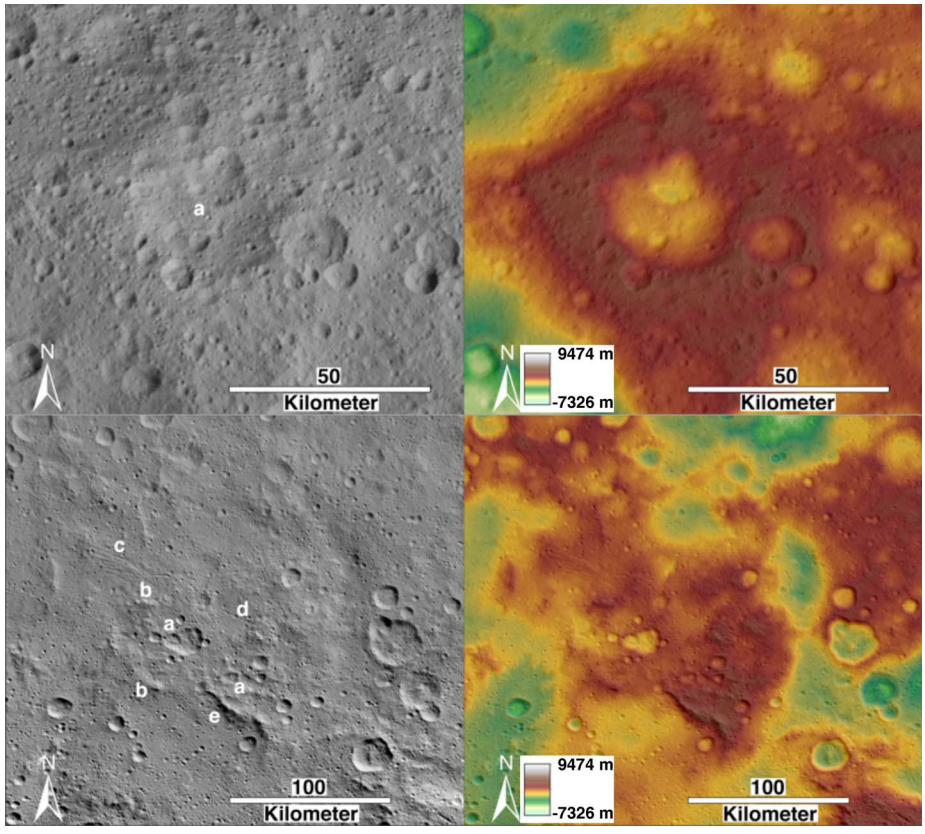

Fig. 4. Detailed views of areas A and B. (**Top**) Area A, as seen from the HAMO (left) and with superposed color-coded topography (right). The area is characterized by a topographic rise with nested, irregularly shaped depressions (a). (**Bottom**) Area B, as seen from the HAMO (left) and with superposed color-coded topography (right). The area is characterized by a topographic rise with nested, irregularly shaped depressions (a); linear settings of domelike structures (b); a graben system (c); a >50-km-long, straight, pitted fracture (d); and the steep cliff of Niman Rupes (e). The topographic range in both DEMs is from −7326 to 9474 m.

mixture. Hence, the observed simple-to-complex crater transition diameters on Ceres are most consistent with an ice-bearing upper crust or a material mixture of similar viscosity. Together with the apparent absence of widespread viscous relaxation, the relatively small measured transition diameters indicate that, paradoxically, Ceres' crust is weak (icelike) on the time scale of crater formation and modification but relatively strong over longer, geologic time scales. At a temperature of 160 K, it has been estimated that the upper tens of kilometers of a "weak" (icelike) crust have a viscosity of 10^{22} Pa·s. The upper limit is less well constrained and is estimated to be on the order of 10^{25} to 10^{27} Pa·s (*26*). Thus, the crust of Ceres is not as strong as pure rock.

Spatial distribution of craters

On the basis of Survey orbit data (400 m per pixel), we globally (95%) mapped all impact craters down to a few kilometers in size. Several coauthors have independently produced crater catalogs (see supplementary materials) on the basis of images from different mission phases [Approach, pre-Survey, and Survey (*5*)] that all agree well with each other concerning the absolute number of craters in different diameter ranges. Figure 3 and Table 1 show craters larger than 20 km, which are clearly visible at the given FC pixel scale, to avoid effects of incomplete counts, terrain effects, and secondary cratering. All catalogs show an absence of craters larger than 300 km, while low-pass filtering of the DEM suggests the existence of at least two quasi-circular depressions with diameters of ~570 (125.56°E and 19.60°N) and ~830 km (24.76°W and 0.5°N). Given the uncertainties in the earliest impact flux on Ceres, such basins are consistent with the estimates of de Elía and Di Sisto (*33*), who calculated the number of craters produced by main-belt asteroids as a function of crater diameter. From figure 4 of (*33*), the largest crater produced by asteroids on Ceres has a diameter of ~600 km. The survival of such large basins might hint at limited amounts of viscous relaxation in these areas compared with other areas or relatively young ages of these basins.

Craters are heterogeneously distributed across the surface of Ceres, with the northern hemisphere being more heavily cratered than the southern hemisphere. The lowest crater densities—associated with large, well-preserved impact craters (e.g., Urvara and Yalode)—are located in the southern hemisphere. Additional regions with relatively LCDs are associated with craters Kerwan, Ezinu, Vinotonus, and two unnamed craters southeast (155 km, 4.0°E and 38.8°N) and northeast (110 km, 14.0°E and 54.7°N) of Oxo crater (10 km) (Fig. 3). Plausible reasons for the LCD terrains include viscous relaxation (*4*, *34*), ejecta burial (*35*), and seismic shaking (*36*). Because the LCD terrain sometimes extends across a large latitude range (e.g., Kerwan: ~30°N to 46°S; Urvara and Yalode: ~18°N to 75°S), its spatial distribution is inconsistent with simple relaxation driven by warmer equatorial temperatures. Instead, because the LCD terrain is associated with large craters, we propose that impact-driven resurfacing is the more likely process of formation, although we cannot completely rule out an endogenic origin. Such an endogenic origin might be plausible for two LCD terrains [i.e., area A (349.5°E and 22.5°N) and area B (54.2°E and 23.3°S)] (Fig. 3). Both areas appear to be positive topographic structures with central depressions. Area A is a ~100-km-wide, ~6-km-high topographic rise and exhibits heavily eroded nested pits that are up to ~2 km deep (Fig. 4). Area B is a ~130-km-wide topographic rise and is characterized by nested ~7- to 20-km pits with different depths, chains of ~5- to 20-km domelike structures, and a ~15-by-60–km swarm of subparallel ~1- to 2-km-wide east-west oriented graben-like valleys (i.e., rilles) (Fig. 4). If these areas were resurfaced by the deposition of endogenic material, its thickness must be on the order of ~700 to 800 m to obliterate 20-km-large craters (*27*). Ahuna Mons, a possible cryovolcanic construct (*37*), is located in an area that is more heavily cratered than the immediate vicinity, implying that potential cryovolcanism did not substantially resurface that region.

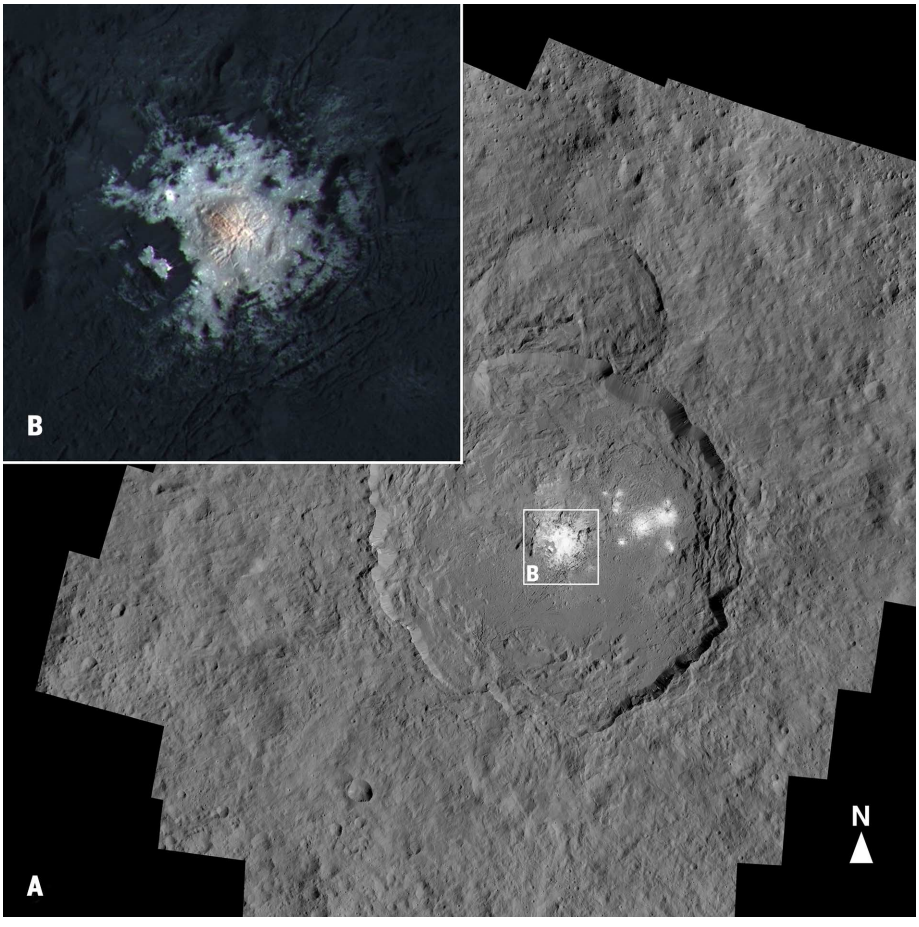

Fig. 5. Occator crater. Occator is a 92-km-diameter, 4-km-deep impact crater that contains the brightest spot on Ceres. Panel (**A**) shows a Low-Altitude Mapping Orbit FC mosaic indicating the location of enhanced-color inset (**B**), which shows the sharply defined bright spot associated with a central dome with a radial fracture pattern surrounded by concentric fractures.

Table 1. Frequency of craters per diameter bin of the crater catalog shown in Fig. 3.

Crater diameter (km)	Number of craters
20–25	137
25–30	98
30–35	67
35–40	52
40–45	27
45–50	34
50–55	24
55–60	18
60–65	10
65–70	17
70–75	9
75–80	6
80–85	6
85–90	1
90–100	6
100–120	10
120–150	5
150–200	1
200–300	3

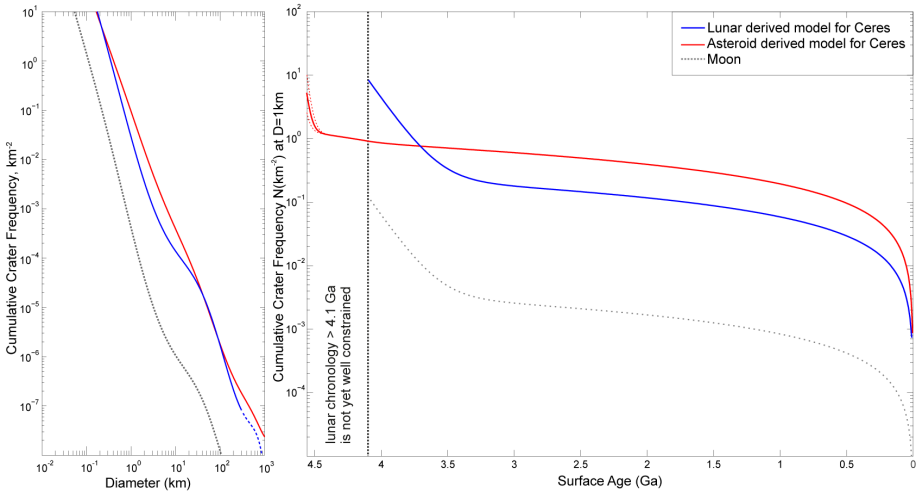

Fig. 6. Production functions and chronology functions for Ceres and the Moon. (**Left**) PFs for the Moon and Ceres, based on the LDM and the ADM. The LDM PF is shown as a dashed line for crater sizes larger than 300 km, which are outside of the valid diameter range of the lunar PF (*44*). (**Right**) CFs for the Moon and Ceres (LDM and ADM). The lunar PF and CF are from (*44*). D, diameter.

A heterogeneous crust is not only indicated by the spatial distribution of impact craters but also by FC and VIR color data (*10*, *38*). In FC images, the surface of Ceres is rather dark, but some craters (such as Occator) exhibit a high albedo and a central pit spectrum that has been interpreted as hydrated magnesium sulfate (*38*) or sodium carbonates mixed with a dark component, small amounts of phyllosilicates, ammonium carbonates, and/or ammonium chloride (Fig. 5) (*39*). False-color composites and VIR spectral data reveal compositional differences on the surface that reflect crustal heterogeneities at all scales (*10*, *38*, *40*). For example, Occator crater shows the largest diversity in colors, ranging from bright spectrally reddish units (central pit) to dark spectrally convex-shaped units (ejecta). Though local deviations from nearly-neutral spectral slopes in the red-visual spectrum to negative slopes are characteristic at many sites, pronounced positive slopes are almost absent and confined to small exposures (*38*).

Absolute model ages (AMAs)

Crater size-frequency distribution (CSFD) measurements are commonly used to derive relative and AMAs of unsampled planetary surfaces (*41*–*44*). To obtain AMAs from observed CSFDs, two main components are needed: a production function (PF) and a chronology function (CF) (Fig. 6). A PF, which describes the time-average idealized shape of the cumulative size-frequency distribution of craters, is needed to extrapolate the measured CSFD to a distinct reference diameter (e.g., 1 or 10 km), whose cumulative crater frequency can then be used to obtain an AMA from the CF (*41*–*44*), which correlates crater densities with absolute ages. Here we describe two approaches to derive such functions. The lunar-derived model (LDM) adapts the lunar PF and CF to impact conditions on Ceres, taking into account a number of parameters [e.g., impact velocities (Fig. 7), projectile densities, current collision probabilities, and surface gravity] in a similar manner as has been done for Mars and Mercury, among others (*41*). The asteroid-derived model (ADM) derives a PF by scaling the directly observed object size-frequency distribution from the main asteroid belt, extended to sizes smaller than 3 to 5 km by a collisional model (*45*), to the resulting size-frequency distribution of craters on Ceres using similar cerean target parameters as the LDM (*46*–*48*). A CF for the ADM is derived independently from lunar observation and is exclusively based on collision rates as they are observed in the current asteroid belt, in combination with dynamical models of the early evolution of the asteroid belt (*49*, *50*). The two approaches are described in detail in the Materials and methods section.

Both approaches have their advantages: For instance, the PF from the ADM is at least partly derived from direct observations of objects in the main asteroid belt, and the CF benefits from the latest dynamical models of the asteroid belt (*49*, *50*). On the other hand, assuming that the asteroid belt shows the same declining flux as the Moon, the functions from the LDM profit from the lunar PF being based on direct crater observations, even down to the smallest crater diameter range, and from the absolute calibration of the lunar CF using radiometric ages from Apollo and Luna samples. However, both approaches also have uncertainties. For example, the LDM assumes that the flux of the impacting projectiles in the asteroid belt exhibits the same characteristics as on the Moon, including an exponential decay of the flux from at least ~4.1 billion to ~3 billion years ago (Ga). This would lead to a massive primordial main belt, resulting in high numbers of expected impact basins on Ceres' ancient surface, which is inconsistent with current observations but might partially be explained by relaxation processes. On the other hand, the PF used in the ADM can only be directly derived from the size-frequency distribution (SFD) of projectiles (>~3 to 5 km) in the asteroid belt, resulting in crater diameters of ~20 to 30 km, whereas the portion of the PF for smaller diameters has to be extrapolated due to incomplete observations of smaller bodies (potential projectiles) in the asteroid belt. Furthermore, the CF from the ADM cannot be properly calibrated using radiometric ages from planetary samples and depends on the assumed parameters of the dynamical models.

We applied both LDM and ADM to CSFDs of the smooth deposits around Kerwan crater because unraveling the geologic history of the Kerwan region is essential for our understanding of past and recent processes on Ceres' surface (Fig. 8). In addition, the region shown at left in Fig. 8, which corresponds to about 9 to 10% of the cerean surface, was selected because it represents a large, first-order homogeneous unit, which is necessary for reliable CSFD-based age determinations. CSFDs were independently determined by four team members and agree well with each other, implying that craters were reliably identified and their numbers and sizes consistently measured. By applying the LDM to these CSFD measurements, we derive an AMA of ~720 My; we obtain a somewhat younger AMA of ~550 My when applying the ADM (Fig. 8).

We also used the LDM and ADM to estimate the potential formation ages of the two ~570- and ~830-km-large depressions detected in the filtered topography data. Assuming that these depressions are impact structures formed by single impacts, their sizes are comparable with those of the Rheasilvia and Veneneia basins on Vesta if scaled to Ceres size. Like Rheasilvia and Veneneia on Vesta, the quasi-circular depressions on Ceres might represent the two youngest, surviving, large basinlike features on Ceres. If correct, based on the LDM we would expect the formation of the smaller feature within the past 3.5 billion years (Gy) and the formation of the larger feature within the past 3.7 Gy, consistent with the formation of the youngest basins on other planetary bodies (Moon, Mars), as well as on Vesta [lunar-like model (*42*)]. In the ADM, the formation of the smaller feature would be expected within the past 2.8 Gy, whereas the larger feature probably formed shortly after the advent of the solar system. The ages of the two depressions are relatively close together in the LDM, as the chronology curve has a steep slope in that age range. In contrast, the chronology curve in the ADM is much flatter until ~4.4 Ga before rising steeply; hence, the ages of the two basins in the ADM are more widely separated (Fig. 6).

Conclusions

Ceres is a heavily cratered object that shows a wide variety of impact sizes and morphologies, although we observe an absence of large (>300 km) craters. The small amount of observed relaxation suggests that the crust contains less ice and/or may be thicker than predicted by some models. Craters are heterogeneously distributed across the surface, indicating crustal heterogeneities and a complex geologic evolution of Ceres' crust and upper mantle, an interpretation supported by FC

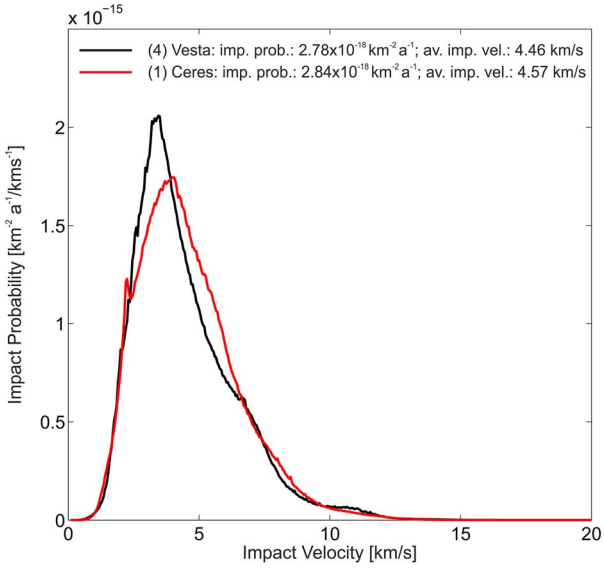

Fig. 7. Intrinsic impact probability with respect to impact velocity for Ceres and Vesta. The calculation is for ≥5-km bodies that cross the orbits of Vesta and Ceres (*62*). Details of the calculation are provided in the Materials and methods section.

and VIR color data. Dating the smooth deposits around Kerwan, one of the largest and most relaxed craters on Ceres, revealed young retention ages of 550 and 720 My, indicating that at least some geologic activity took place in the recent history of Ceres.

Materials and methods

Lunar-derived model (LDM)

The determination of AMAs at Ceres on the basis of the LDM, follows the approach of (*42*, *51*, *52*). The first publication describes in detail the methodology of converting the lunar chronology system (crater PF and CF) to main-belt asteroids of rocky composition. The authors reproduce results of earlier publications (*53*–*55*) and link the AMA related to the formation of the Rheasilvia basin on Vesta to the youngest and most prominent reset event of brecciated HED meteorites about 3.5 Ga (*56*). Here we extend that approach to Ceres, whose surface composition (*8*, *10*, *38*) and related models of thermochemical evolution (*2*, *3*, *18*) are consistent with high abundances of volatile materials. The remarkable similarities in crater morphologies between Ceres and saturnian icy satellites may be a result of similar rheologic characteristics of the target material as well as similar surface gravities.

For converting the lunar cratering record to the impact conditions on Ceres we use the scaling laws by (*57*) (Eqs. 1 to 3) that are designed for scaling between projectile and crater sizes of nonporous, zero-friction rocks.

$$C_D = \left[1.16\left(\frac{\delta}{\rho}\right)^{\frac{1}{3}}(v\sin(\alpha))^{0.44}\right]^{1/0.78} \quad (1)$$

$$\frac{D_t}{D_P} = \frac{C_D}{[g(D_{sg}+D_t)]^{0.282}} \quad (2)$$

$$D_t = D_{SC}^{0.15} D^{0.85} \quad (3)$$

Equations 1 and 2 represent the Ivanov scaling laws (*57*). Equation 3 is only used for converting between sizes of complex and transient craters. Following (*51*), we assume that the sizes of simple bowl shaped craters are similar to transient crater sizes, thus, neglecting potential collapse of such craters, which would result in an enlargement of the final crater when compared to the transient diameter. In these equations, the variables are defined as: D, observed crater diameter; D_t, transient crater diameter; D_P, projectile diameter; g, surface gravity of target body; δ, projectile density; ρ, target density; v, impact velocity; α, impact angle; D_{sg}, strength to gravity transition crater diameter; D_{SC}, simple to complex transition crater diameter.

Key parameters in the used scaling laws are the transition size from simple-to-complex craters and the transition size from the strength to gravity scaling regime. Both parameters scale inversely with surface gravity for icy and rocky bodies but are offset between both body types (*27*, *51*, *58*, *59*). Hence, scaling the lunar cratering record to icy bodies requires correction for the different scaling behavior in rocky and icy target materials. In a previous study (*60*), the cerean crater PF has been predicted before high-resolution imaging data were available. In that approach the strength-to-gravity crater diameter as well as the surface gravity of Ceres were incorrectly adjusted in a way as if Ceres is a rocky body with a simple-to-complex transition crater diameter of ~12 km. High-resolution crater measurements of Ceres acquired subsequently did follow the predicted PF very closely. Although this approach resulted in an agreement between theoretical and observed crater distribution, it severely underestimated crater sizes for a given projectile size, which resulted in a too low estimation for the projectile flux.

Here, we present a more sophisticated approach in which the upper limit for the cerean strength-to-gravity transition can be estimated by the size of the largest stable crater with Eq. 4 (*61*).

$$\rho g D_{sg} \le 13.5 Y_0 \quad (4)$$

With a simple-to-complex transition of 10 km and Eq. 5 (*61*), we get for Y_0 a value of about 0.15 MPa.

$$\frac{27 Y_0}{\rho g} \le D_{SC} \quad (5)$$

Thus, for Ceres we find a value of ~5 km as upper limit for D_{sg} using values from table S1.

In order to find the correct value, we reduced D_{sg} in Eq. 2 until we arrived at a solution that best resembled the shape of the crater PF of (*60*). This resulted in a D_{sg} of 1.75 km and also implies a value for Y_0 of about 50 kPa, which is the average material cohesion during the process of crater formation.

The PF is a model of cumulative crater frequencies in dependence of crater diameters. It should resemble the observed crater size-frequency distribution of the body measured on surfaces undisturbed by geological processes or additional secondary craters. Table S2 gives the coefficients of an 11th-degree polynomial equation (Eq. 6) (*44*, *52*) that describes the shape of the LDM crater PFs for the Moon and Ceres.

$$\log N_{cum} = a_0 + a_1\log(D) + a_2(\log(D))^2 + \ldots + a_{11}(\log(D))^{11} \quad (6)$$

The CF relates measured cumulative crater frequencies to AMAs using a crater reference diameter, typically N(1). For estimates of the current intrinsic collision probability of Ceres, we follow the approach of (*62*) and use orbital statistics of Ceres crossing asteroids of ≥5 km diameter. This analysis gives an intrinsic impact probability of 2.84×10^{-18} km^{-2} a^{-1} and an average impact velocity of about 4.57 km/s (Fig. 7). The conversion of collision probabilities into a lunar-like chronology is detailed by (*42*) for the case of Vesta.

Table S3 gives the coefficients of the CF with exponential smooth decay for ages older than about 3.5 Gy (Eq. 7) (*41*) for the Moon, Vesta, and Ceres. For ages older than 4.1 Gy, the cratering history of the Moon is still ambiguous (*63*). Therefore, the given functions may only be used with great caution for older ages.

$$N_{cum}(D \ge 1\text{km}) = C_1(e^{C_2 t} - 1) + C_3 t \quad (7)$$

The presented LDM chronology system for Ceres (Fig. 6) is an estimation of the cratering history averaged over billions of years. A break up event inside the main belt could cause higher impact rates on Ceres as well as on other asteroids for a short period of time. If such an event occurred recently, young areas may appear older than they actually are. Very old areas are less affected, because short fluctuations in impact rate average out over time. In addition to statistical errors that arise from fitting the crater PF to the measured crater size-frequency distribution, there might be systematic errors present as well. Such errors could be related to the shape of the derived crater PF or the estimation of intrinsic collision probabilities.

Asteroid-derived model (ADM)

The ADM uses the chronology curve derived for Vesta by (*43*), adjusted for the different production rates of craters on Ceres (Fig. 6). Briefly, the chronology curve is based on the best current models of main-belt dynamical and collisional history, accounting for two main phases: (i) an initial sharp decline in mass of the belt during the ~100 Ma immediately following the formation of the solar system (*64*–*66*); and (ii) the subsequent depletion of the belt by a factor of ~4

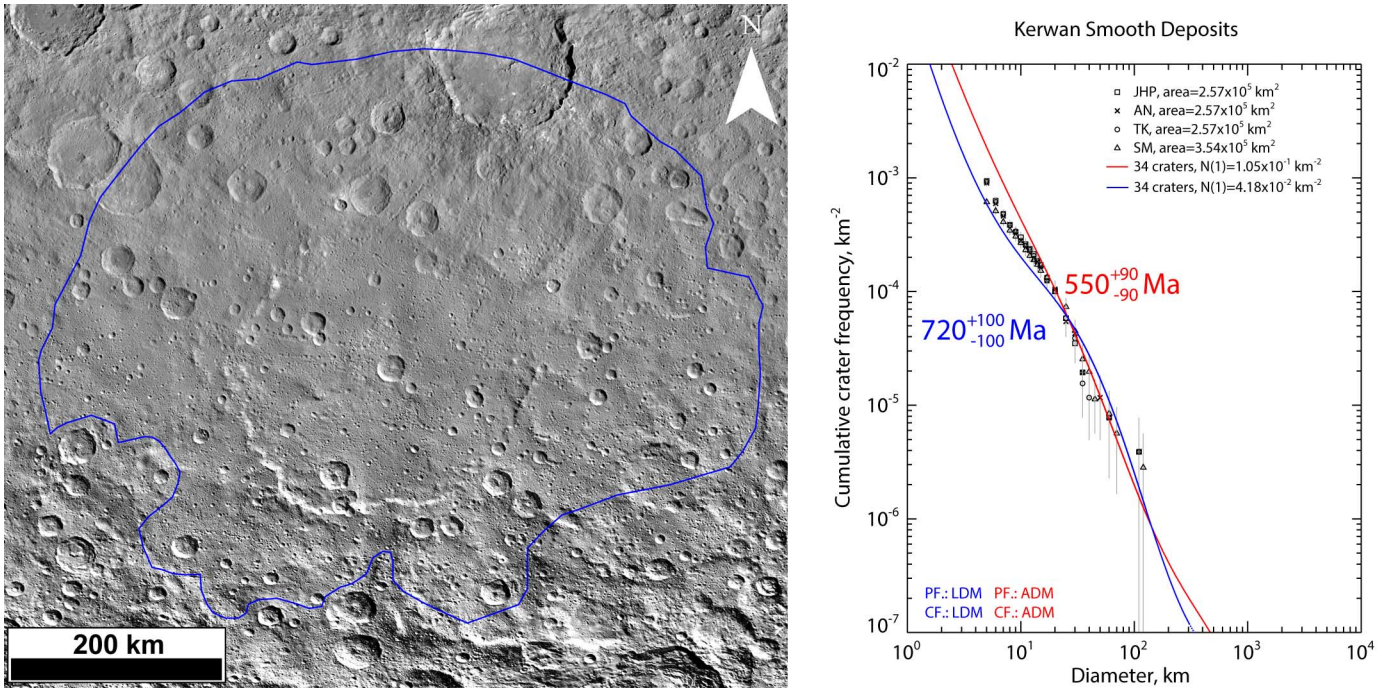

Fig. 8. Age determination for the Kerwan impact crater on Ceres. (**Left**) The HAMO mosaic shows the smooth deposits associated with Kerwan crater. The area for which we (J.H.P., A.N., S.M.) performed CSFD measurements is outlined in blue. The count area of S.M. overlaps this area and extends farther to the west. (**Right**) CSFD plot for the area shown at left. Several coauthors (J.H.P., A.N., T.K., and S.M.) independently performed CSFD measurements. To derive AMAs, we used the PFs and CFs of the LDM (blue) and the ADM (red).

during the time of the Late Heavy Bombardment due to secular resonance sweeping (*49*) and the loss of dynamically unstable asteroids (*50*). It is important to note that while the chronology curve for the asteroid belt derived in this manner differs significantly in shape from the lunar chronology curve (and hence also the LDM curve) (Fig. 6), there is no a priori reason to think that they should be the same (which is a central assumption of the LDM). In fact, Morbidelli *et al.* (*63*) show that the asteroid flux into the terrestrial planet region due to dynamical depletion processes within the asteroid belt results in an impact flux on the Moon consistent with the lunar chronology of (*41*, *52*, *67*).

To apply the ADM chronology curve to Ceres, the current production rate of craters on Ceres must be calculated. The chronology curve allows for the extrapolation of the impact rate back in time. The crater PF is calculated adopting a model main-belt SFD, an asteroid impact velocity distribution based on current asteroids larger than 50 km crossing the orbit of Ceres, and a crater scaling law from (*68*). It should be noted that the main-belt SFD is taken from (*45*), which provides a good fit to the observed main-belt SFD down to the completeness limit of ~3 km. The resulting PF also has produced a reasonable match to crater counts on young surfaces on Vesta (*46*). Further details of the model can be found in (*46*, *48*, *69*).

REFERENCES AND NOTES

1. C. T. Russell, C. A. Raymond, The Dawn mission to Vesta and Ceres. *Space Sci. Rev.* **163**, 3–23 (2011). doi: 10.1007/s11214-011-9836-2
2. J. C. Castillo-Rogez, T. B. McCord, Ceres' evolution and present state constrained by shape data. *Icarus* **205**, 443–459 (2010). doi: 10.1016/j.icarus.2009.04.008
3. T. B. McCord, C. Sotin, Ceres: Evolution and current state. *J. Geophys. Res.* **110**, E05009 (2005). doi: 10.1029/2004JE002244
4. M. T. Bland, Predicted crater morphologies on Ceres: Probing internal structure and evolution. *Icarus* **226**, 510–521 (2013). doi: 10.1016/j.icarus.2013.05.037
5. C. T. Russell *et al.*, Dawn arrives at Ceres: Exploration of a small, volatile-rich world. *Science* **353**, aaf4219 (2016).
6. L. A. Lebofsky, M. A. Feierberg, A. T. Tokunaga, H. P. Larson, J. R. Johnson, The 1.7- to 4.2- μm spectrum of asteroid 1 Ceres: Evidence for structural water in clay minerals. *Icarus* **48**, 453–459 (1981). doi: 10.1016/0019-1035(81)90055-5
7. T. V. V. King, R. N. Clark, W. M. Calvin, D. M. Sherman, R. H. Brown, Evidence for ammonium-bearing minerals on ceres. *Science* **255**, 1551–1553 (1992). doi: 10.1126/science.255.5051.1551; pmid: 17820166
8. A. S. Rivkin, E. L. Volquardsen, B. E. Clark, The surface composition of Ceres: Discovery of carbonates and iron-rich clays. *Icarus* **185**, 563–567 (2006). doi: 10.1016/j.icarus.2006.08.022
9. R. E. Milliken, A. S. Rivkin, Brucite and carbonate assemblages from altered olivine-rich materials on Ceres. *Nat. Geosci.* **2**, 258–261 (2009). doi: 10.1038/ngeo478
10. M. C. De Sanctis *et al.*, Ammoniated phyllosilicates with a likely outer solar system origin on (1) Ceres. *Nature* **528**, 241–244 (2015). doi: 10.1038/nature16172; pmid: 26659184
11. C. R. Chapman, J. W. Salisbury, Comparisonos of meteorite and asteroid spectral reflectivities. *Icarus* **19**, 507–522 (1973). doi: 10.1016/0019-1035(73)90078-X
12. T. B. McCord, M. J. Gaffey, Asteroids: Surface composition from reflection spectroscopy. *Science* **186**, 352–355 (1974). doi: 10.1126/science.186.4161.352; pmid: 17839866
13. M. C. De Sanctis *et al.*, The VIR spectrometer. *Space Sci. Rev.* **163**, 329–369 (2011). doi: 10.1007/s11214-010-9668-5
14. T. H. Prettyman *et al.*, Dawn's Gamma Ray and Neutron Detector. *Space Sci. Rev.* **163**, 371–459 (2011). doi: 10.1007/s11214-011-9862-0
15. H. Sierks *et al.*, The Dawn Framing Camera. *Space Sci. Rev.* **163**, 263–327 (2011). doi: 10.1007/s11214-011-9745-4
16. P. Schenk *et al.*, "An ice-rich mantle on Ceres from Dawn mapping of central pit and peak crater morphologies," abstract P53E-2186, presented at the American Geophysical Union Fall Meeting, San Francisio, CA, 14 to 18 December 2015.
17. D. L. Buczkowski *et al.*, The geomorphology of Ceres. *Science* **353**, aaf4332 (2016).
18. T. McCord, J. Castillo-Rogez, A. Rivkin, Ceres: Its origin, evolution and structure and Dawn's potential contributions. *Space Sci. Rev.* **163**, 63–76 (2011). doi: 10.1007/s11214-010-9729-9
19. J. C. Castillo-Rogez, Ceres – Neither a porous nor a salty ball. *Icarus* **215**, 599–602 (2011). doi: 10.1016/j.icarus.2011.08.007
20. P. C. Thomas *et al.*, Differentiation of the asteroid Ceres as revealed by its shape. *Nature* **437**, 224–226 (2005). doi: 10.1038/nature03938; pmid: 16148926
21. R. Jaumann *et al.*, Vesta's shape and morphology. *Science* **336**, 687–690 (2012). doi: 10.1126/science.1219122; pmid: 22582254
22. F. Preusker *et al.*, Stereo topographic models of Mercury after three MESSENGER flybys. *Planet. Space Sci.* **59**, 1910–1917 (2011). doi: 10.1016/j.pss.2011.07.005
23. F. Preusker *et al.*, Dawn at Ceres – Shape models and rotational state. *Lunar Planet. Sci. Conf.* **47**, abstract 1954 (2016).
24. P. O. Hayne, O. Aharonson, Thermal stability of ice on Ceres with rough topography. *J. Geophys. Res.* **120**, 1567–1584 (2015). doi: 10.1002/2015JE004887
25. M. Y. Zolotov, On the composition and differentiation of Ceres. *Icarus* **204**, 183–193 (2009). doi: 10.1016/j.icarus.2009.06.011
26. M. T. Bland *et al.*, Composition and structure of the shallow subsurface of Ceres as revealed by crater morphology. *Nat. Geosci.* **9**, 538–542 (2016). doi: 10.1038/ngeo2743
27. R. J. Pike, "Geometric interpretation of lunar craters" (U.S. Government Printing Office, 1980).
28. O. L. White, P. M. Schenk, A. J. Dombard, Impact basin relaxation on Rhea and Iapetus and relation to past heat flow. *Icarus* **223**, 699–709 (2013). doi: 10.1016/j.icarus.2013.01.013
29. P. M. Schenk *et al.*, "Ages and interiors: The cratering record of the Galilean satellites," in *Jupiter*, F. Bagenal, T. Dowling, W. McKinnon, Eds., (Cambridge Univ. Press, 2004), pp. 427–456.
30. R. G. Kraus, L. E. Senft, S. T. Stewart, Impacts onto H_2O ice: Scalling laws for melting, vaporization, excavation, and final crater size. *Icarus* **214**, 724–738 (2011). doi: 10.1016/j.icarus.2011.05.016

31. R. P. Di Sisto, M. Zanardi, The production of craters on the mid-sized Saturnian satellites by Centaur objects. *Astron. Astrophys.* **553**, A79 (2013). doi: 10.1051/0004-6361/201220568
32. G. Steinbrügge, A. Stark, H. Hussmann, F. Sohl, J. Oberst, Measuring tidal deformations by laser altimetry: A performance model for the Ganymede Laser Altimeter. *Planet. Space Sci.* **117**, 184–191 (2015). doi: 10.1016/j.pss.2015.06.013
33. G. C. de Elía, R. P. Di Sisto, Impactor flux and cratering on Ceres and Vesta: Implications for the early solar system. *Astron. Astrophys.* **534**, A129 (2011).
34. E. M. Parmentier, J. W. Head, Viscous relaxation of impact craters on icy planetary surfaces: Detrermination of viscosity variation with depth. *Icarus* **47**, 100–111 (1981). doi: 10.1016/0019-1035(81)90095-6
35. D. E. Wilhelms, "The geologic history of the Moon" (U.S. Geological Survey Professional Paper 1348, 1987).
36. J. E. Richardson Jr., H. Melosh, R. Greenberg, D. Obrien, The global effects of impact-induced seismic activity on fractured asteroid surface morphology. *Icarus* **179**, 325–349 (2005). doi: 10.1016/j.icarus.2005.07.005
37. O. Ruesch *et al*., Cryo-volcanism on Ceres. *Science* **353**, aaf4286 (2016).
38. A. Nathues *et al*., Sublimation in bright spots on (1) Ceres. *Nature* **528**, 237–240 (2015). doi: 10.1038/nature15754; pmid: 26659183
39. M. C. De Sanctis *et al*., Bright carbonate deposits as evidence of aqueous alteration on (1) Ceres. *Nature* **536**, 54–57 (2016). doi: 10.1038/nature18290; pmid: 27362221
40. E. Ammannito *et al*., Distribution of phyllosilicates on the surface of Ceres. *Science* **353**, aaf4279 (2016).
41. G. Neukum, B. A. Ivanov, W. K. Hartmann, Cratering records in the inner solar system in relation to the lunar reference system. *Space Sci. Rev.* **96**, 55–86 (2001). doi: 10.1023/A:1011989004263
42. N. Schmedemann *et al*., The cratering record, chronology and surface ages of (4) Vesta in comparison to smaller asteroids and the ages of HED meteorites. *Planet. Space Sci.* **103**, 104–130 (2014). doi: 10.1016/j.pss.2014.04.004
43. D. P. O'Brien *et al*., Constraining the cratering chronology of Vesta. *Planet. Space Sci.* **103**, 131–142 (2014). doi: 10.1016/j.pss.2014.05.013
44. G. Neukum, "Meteoritenbombardement und Datierung planetarer Oberflächen," thesis, University of Munich (1983).
45. W. F. Bottke Jr. *et al*., Linking the collisional history of the main asteroid belt to its dynamical excitation and depletion. *Icarus* **179**, 63–94 (2005). doi: 10.1016/j.icarus.2005.05.017
46. S. Marchi *et al*., Small crater populations on Vesta. *Planet. Space Sci.* **103**, 96–103 (2014). doi: 10.1016/j.pss.2013.05.005
47. S. Marchi *et al*., High-velocity collisions from the lunar cataclysm recorded in asteroidal meteorites. *Nat. Geosci.* **6**, 303–307 (2013). doi: 10.1038/ngeo1769
48. S. Marchi *et al*., The violent collisional history of asteroid 4 Vesta. *Science* **336**, 690–694 (2012a). doi: 10.1126/science.1218757; pmid: 22582255
49. A. Morbidelli, R. Brasser, R. Gomes, H. F. Levison, K. Tsiganis, Evidence from the asteroid belt for a violent past evolution of Jupiter's orbit. *Astron. J.* **140**, 1391–1401 (2010). doi: 10.1088/0004-6256/140/5/1391
50. D. A. Minton, R. Malhotra, Dynamical erosion of the asteroid belt and implications for large impacts in the inner solar system. *Icarus* **207**, 744–757 (2010). doi: 10.1016/j.icarus.2009.12.008
51. B. A. Ivanov, Mars/Moon cratering rate ratio estimates. *Space Sci. Rev.* **96**, 87–104 (2001). doi: 10.1023/A:1011941121102
52. G. Neukum, B. A. Ivanov, "Crater size distributions and impact probabilities on Earth from lunar, terrestrial-planet, and asteroid cratering data," in *Hazard Due to Comets and Asteroids*, T. Gehrels, Ed. (Univ. of Arizona Press, 1994), pp. 359–416.
53. C. R. Chapman, J. Veverka, M. J. S. Belton, G. Neukum, D. Morrison, Cratering on Gaspra. *Icarus* **120**, 231–245 (1996). doi: 10.1006/icar.1996.0048
54. C. R. Chapman *et al*., Cratering on Ida. *Icarus* **120**, 77–86 (1996). doi: 10.1006/icar.1996.0038
55. S. Marchi *et al*., The cratering history of asteroid (21) Lutetia. *Planet. Space Sci.* **66**, 87–95 (2012). doi: 10.1016/j.pss.2011.10.010
56. D. D. Bogard, K-Ar ages of meteorites: Clues to parent-body thermal histories. *Chemie der Erde – Geochemistry* **71**, 207–226 (2011). doi: 10.1016/j.chemer.2011.03.001
57. S. C. Werner, B. A. Ivanov, "Exogenic dynamics, cratering, and surface ages," in *Treatise on Geophysics* (Elsevier, ed. 2, 2015), vol. 10, pp. 327–365.
58. P. M. Schenk, Ganymede and Callisto: Complex crater formation and planetary crusts. *J. Geophys. Res.* **96**, 15635–15664 (1991). doi: 10.1029/91JE00932
59. J. M. Moore *et al*., Impact features on Europa: Results of the Galileo Europa Mission (GEM). *Icarus* **151**, 93–111 (2001). doi: 10.1006/icar.2000.6558
60. N. Schmedemann *et al*., A preliminary chronology for Ceres. *Lunar Planet. Sci. Conf.* **46**, abstract 1418 (2015).
61. H. J. Melosh, *Impact Cratering – A Geologic Process* (Oxford Univ. Press, 1989).
62. W. F. Bottke Jr., M. C. Nolan, R. Greenberg, R. A. Kolvoord, Velocity distributions among colliding asteroids. *Icarus* **107**, 255–268 (1994). doi: 10.1006/icar.1994.1021
63. A. Morbidelli, S. Marchi, W. F. Bottke, D. A. Kring, A sawtooth-like timeline for the first billion years of lunar bombardment. *Earth Planet. Sci. Lett.* **355–356**, 144–151 (2012). doi: 10.1016/j.epsl.2012.07.037
64. G. W. Wetherill, An alternative model for the formation of the asteroids. *Icarus* **100**, 307–325 (1992). doi: 10.1016/0019-1035(92)90103-E
65. J. Petit *et al*., The primordial excitation and clearing of the asteroid belt. *Icarus* **153**, 338–347 (2001). doi: 10.1006/icar.2001.6702
66. D. P. O'Brien, A. Morbidelli, W. F. Bottke, The primordial excitation and clearing of the asteroid belt—Revisited. *Icarus* **191**, 434–452 (2007). doi: 10.1016/j.icarus.2007.05.005
67. G. Neukum, D. E. Wilhelms, "Ancient lunar impact record," in *Lunar and Planetary Institute Science Conference*, abstracts of Lunar and Planetary Institute (Technical Report 13, 1982), pp. 590–591.
68. K. A. Holsapple, K. R. Housen, A crater and its ejecta: An interpretation of Deep Inpact. *Icarus* **187**, 345–356 (2007). doi: 10.1016/j.icarus.2006.08.029
69. S. Marchi *et al*., The cratering history of asteroid (2867) Steins. *Planet. Space Sci.* **58**, 1116–1123 (2010). doi: 10.1016/j.pss.2010.03.017

ACKNOWLEDGMENTS

We thank the Dawn team for the development, cruise, orbital insertion, and operations of the Dawn spacecraft at Ceres. C.T.R. is supported by the Discovery Program through contract NNM05AA86C to the University of California, Los Angeles. A portion of this work was performed at the Jet Propulsion Laboratory, California Institute of Technology, under contract with NASA. J.H.P. and H.H. are supported by the DLR Space Administration on behalf of the German Federal Ministry for Economic Affairs and Energy, grant 50 OW 1502 (DAWN). M.T.B. was supported by NASA's Dawn at Ceres Guest Investigator Program. Dawn data are archived with the NASA Planetary Data System. FC data may be obtained at http://sbn.psi.edu/pds/resource/dwncfc2.html. VIR spectral data may be obtained at http://sbn.psi.edu/pds/resource/dwncvir.html. GRaND data may be obtained at http://sbn.psi.edu/pds/resource/dwncgrd.html. The Ceres crater catalog described in the text and measurements of the transition diameter from simple to complex craters are available in the supplementary materials. As chair of the Dawn chronology working group, H.H. coordinated the contributions and prepared the manuscript. S.M. provided input on the distribution of craters and the PFs and CFs. N.S., A.Ne., T.K., and D.P.O. also provided input for the PFs and CFs. P.S. and T.P. made contributions to the simple-to-complex transition. J.H.P. performed CSFD measurements and helped with preparing the manuscript. A.Na. provided the description of color properties. A.I.E., R.R.F., R.S.P., F.P., J.C.C.-R., M.T.B., and C.A.R. contributed their expertise in geophysical modeling. D.A.W., R.J., B.S., D.L.B., and O.R. helped with manuscript preparation and provided useful comments and suggestions. C.T.R. is the Dawn principal investigator and guided the research.

SUPPLEMENTARY MATERIALS

www.sciencemag.org/content/353/6303/aaf4759/suppl/DC1
Tables S1 to S3
Reference (*70*)
Data S1

14 February 2016; accepted 29 July 2016
10.1126/science.aaf4759

Cratering on Ceres: Implications for its crust and evolution
H. Hiesinger, S. Marchi, N. Schmedemann, P. Schenk, J. H. Pasckert, A. Neesemann, D. P. O'Brien, T. Kneissl, A. I. Ermakov, R. R. Fu, M. T. Bland, A. Nathues, T. Platz, D. A. Williams, R. Jaumann, J. C. Castillo-Rogez, O. Ruesch, B. Schmidt, R. S. Park, F. Preusker, D. L. Buczkowski, C. T. Russell and C. A. Raymond
(September 1, 2016)
Science **353** (6303), . [doi: 10.1126/science.aaf4759]

Editor's Summary

Science (print ISSN 0036-8075; online ISSN 1095-9203) is published weekly, except the last week in December, by the American Association for the Advancement of Science, 1200 New York Avenue NW, Washington, DC 20005.